Met. Mater. Int., Vol. 17, No. 5 (2011), pp. 755~763
doi: 10.1007/s12540-011-1010-6 Published 27 October 2011

Fabrication of Single Crystalline Diamond Reinforced Aluminum Matrix Composite by Powder Metallurgy Route

Hansang Kwon[1,*], Marc Leparoux[1], Jean-Marc Heintz[2], Jean-François Silvain[2], and Akira Kawasaki[3]

[1]Laboratory of Advanced Materials Processing, Empa-Swiss Federal Laboratories for Materials Science and Technology, Feuerwerkerstrasse 39, Thun 3602, Switzerland
[2]Institut de Chimie de la Matiere Condensee de Bordeaux (ICMCB) du CNRS, 87 Avenue du Dr. Albert Schweitzer, Pessac 33608, France
[3]Department of Materials Processing, Graduate School of Engineering, Tohoku University, Sendai 980-8579, Japan

(received date: 14 June 2010 / accepted date: 14 July 2011)

We have successfully fabricated highly densified aluminum (Al)-diamond composite materials by a simple hot press method. The thermal conductivity of the Al-diamond composite materials was measured. These materials had different types, sizes and fractions of diamond. These obtained values were discussed based on theoretically calculated values. The thermal conductivity of the composite materials, measured by Laser-Flash method, was found to have slightly increased compared to that of pure bulk Al. The obtained microstructures of the composite materials showed a lot of cleavage existing in the interface between the Al matrix and the diamond particles, which led to the low increment of the thermal conductivity. Moreover, Al-diamond bulk materials with different sintering temperatures in solid state, liquid phase, and transient region between solid and liquid of Al, have been synthesized.

Keywords: composites, powder processing, sintering, thermal conductivity

1. INTRODUCTION

High thermal conductivity combined with low coefficient of thermal expansion (CTE) heat-sinks has played an important role in achieving high-performance and high reliability for electronic devices and modules [1-6]. Next generation heat sink materials, which are different kinds of thermally adapted materials, have already been suggested and some have been tested on C/C, Cu/diamond, and Cu/CNF. Due to their thermal conductivity, Al and Cu have been considered as candidates for good heat dissipation. However, their high coefficient of thermal expansion (CTE, 18.9×10^{-6} °C and 23×10^{-6} °C) compared to ceramic (Al_2O_3, 8×10^{-6} °C) or silicon chips (4×10^{-6} °C), leads to thermal stress during service and indeed to the catastrophic failure of electric devices [7].

Nowadays complex materials have been an interest for use as thermal management materials because these materials, especially metal-matrix composites (MMCs), have shown an important trait, the possibility to tailor the thermal properties of metals via the addition of an appropriate reinforcement phase [8]. For this reason, Al/SiC, Cu/Mo, and Cu/W composites have been in favor as heat sinks materials for better thermal management of electronic packages [8]. However, these electronic packages, which became very complicated, have led to the demand for microminiaturization and ultra high-performance of electronic packages for industry. Therefore, it is necessary to develop better thermal management materials to keep in step with highly performing electronic packages.

Using a diamond sample with the highest possible thermal conductivity (up to 2200 W/mK at 25 °C), and with all electronic materials at room temperature, combined with a low CTE [9-11]. There have been several attempts to create diamond composites on the basis of the Al and Cu matrix in order to achieve highly performing thermal management materials; it is also hoped that it will be possible to allow for mass production in near-net-shape and to obtain a relatively cheap price using several elaboration methods [5,8,9]. Among these fabrication methods, gas pressure infiltration and squeeze casting infiltration are regarded as the most promising and effective ones [8,9], but these methods have high energy consumption during their fabrication processes.

For the present study, we have investigated the fabrication of Al-diamond composite materials by a simple hot press

*Corresponding author: nanocomposites@hotmail.com

(HP) method. Different types, size and volume fractions of diamond powders have been used in order to investigate the relationship between the thermal properties of the starting materials and the final thermal properties of the densified material. The obtained composite was highly compacted, having a relative density in the range of 95 % to 99 %. Microstructural analysis of the fracture of the composite materials clearly shows good dispersion of the diamond particles but also weak interfacial bonding between the Al matrix and the diamond particles. Moreover, Al-diamond composite materials have been synthesized at different sintering temperatures in the solid state, liquid phase, and transient region between solid and liquid of Al. The obtained microstructures were discussed and correlated with the thermal properties of the composite materials.

2. EXPERIMENTAL PRODUCEDURE

The gas that atomized the Al powder into an irregular shape (purity 99.7 %, average particle size 34 μm, Poudres Hermillon, France) was used for the matrix materials. Single crystal diamond powders, referenced as MBD4, MBD6, and MBD8, and manufactured by Henan Hengxiang Diamond Abrasive CO. Ltd., in China, were used. The Al-diamond mixture powder was prepared with various diamond types (MBD4, 6, and 8), sizes (25-30 μm, 37-44 μm, and 75-88 μm), and fractions (10 vol.%, 30 vol.%, and 50 vol.% diamond) via 3D turbula mixing for 24 h (Turbula Shaker/Mixer Model T2C, Willy A. Bachofen AG, Maschinenfabrik, Germany).

The obtained Al-diamond mixture powders were sintered in a 6 mm diameter graphite mold using a hot-press device with induction heating (Celes, Lautenbach, France). The sintering conditions were at 600 °C, 650 °C, and 700 °C with a heating rate of 50 °C/min, a holding time of 20 min, and a pressure of 50 MPa under Ar/5%H_2 atmosphere. The density of the composite materials was measured by the Archimedes principle. The thermal diffusivity values of the samples with 6 mm in diameter and 2-5 mm thickness, respectively, were measured at room temperature by Laser-Flash method (LFA457 micro flash, NETZSCH, Germany) [12]. A CO_2 laser with power intensity was fixed at 50 W and a maximum pulse impulse of 10 ms. The thermal conductivity (λ) was calculated by the following equation [13]:

$$\lambda = k \times \rho \times Cp \quad (1)$$

where k is the thermal diffusivity of the composite materials, and ρ and Cp are the density and specific heat of the Al-diamond bulk materials, respectively. COMSOL Multiphysics 3.5 software was employed in order to predict the thermal conductivity, coefficient of thermal expansion (CTE), and temperature distribution inside complex electric device structures that include our Al-diamond heat sink materials. The CTE of the samples was measured with a differential dilatometer (DIL 402 CD, NETZSCH, Germany) at a heating rate of 2 °C/min and a heating range from room temperature to 250 °C under an argon atmosphere. The Al-diamond mixture powder and the fracture surfaces of the sintered Al-diamond composite materials were observed by a scanning electron microscope (SEM JSM-840A, JEOL Co. Ltd., Japan) and a transmission electron microscope (TEM, Hitachi200KeV, Japan).

3. RESULTS AND DISCUSSION

Figure 1 shows SEM micrographs of the as-received single crystalline diamonds for the different diamond particle types and sizes. The MBD4 shows smooth and angled surfaces, as can be sen in Figs. 1(a) and (d). The MBD6 shows an almost similar morphology, but presents a rather rougher surface, as can be seen in Figs. 1(b) and (e). In MBD8, the powder surfaces are even rougher, and present themselves as irregularly stair-like on their surface, as can be seen in Figs. 1(c) and (f). As can be seen in Figs. 1(g), (h), and (i) no evolution of the MBD6 surface morphology can be observed for the three ranges of diamond particle size, i.e., 25-30 μm, 37-44 μm, and 75-88 μm.

Figure 2 shows SEM micrographs of the mixture powder of Al-diamond with different types, volume fractions, and sizes of diamond. It was found that the Al-diamond mixture powders with 50 vol.% of MBD4, MBD6, and MBD8 are homogeneously well dispersed, as can be seen in Figs. 2(a), (b), and (c). The volume percentages (50 vol.% and

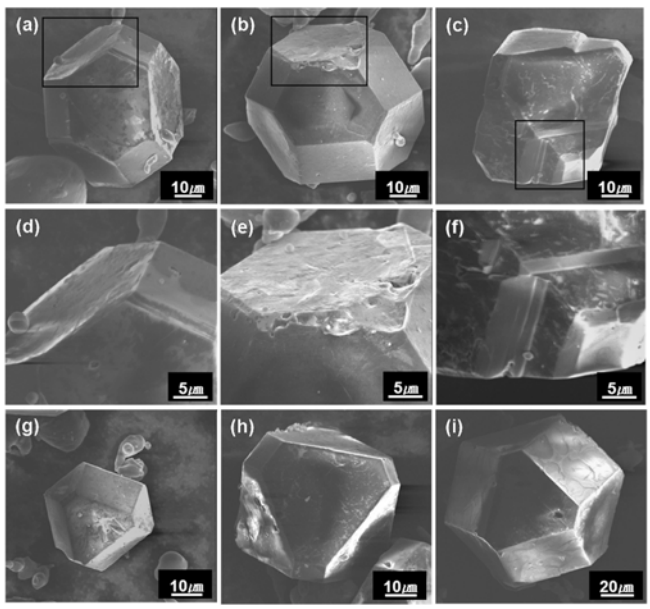

Fig. 1. SEM micrographs of as received diamond particles; (a) MBD4, (b) MBD6, (c) MBD8, (d)-(f) high magnification of them, and (g)-(i) MBD6 in average diameter of 25-30 μm, 37-44 μm, and 75-88 μm.

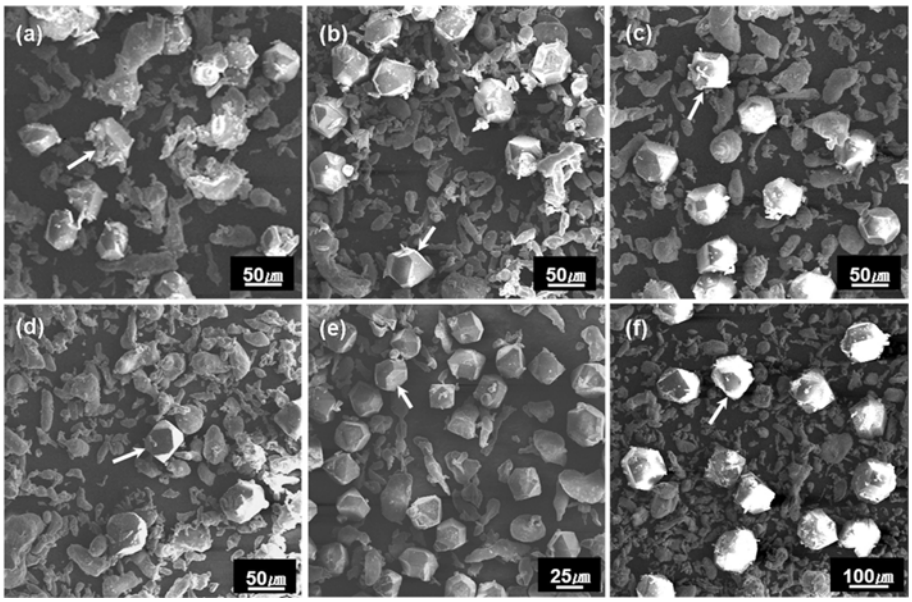

Fig. 2. SEM micrographs of Al-50 vol.% (a) MBD4, (b) MBD6, (c) MBD8, and (d) Al-10 vol.% MBD6 mixture powders. Al-50 vol.% MBD6 with diamond particle size of (e) 25-30 μm and (f) 75-88 μm. The white arrows indicate diamond particles.

10 vol.% of MBD6) did not affect the dispersity of Al-diamond mixture powder, as can be seen in Figs. 2(b) and (d). The quality of the Al-diamond mixture is not affected by the size of the diamond particles (Figs. 2(e) 25-30 μm, (b) 37-44 μm, and (f) 75-88 μm of MBD6). In other words, it is possible to achieve a homogeneously well dispersed Al-diamond mixture powder when using simple turbular mixing.

We have attempted to determine the thermal characteristics of electronic device architecture, which includes our Al-diamond heat sink, by COMSOL Multiphysics 3.5 software. In general, the power semiconductor modules consist of a multi-layer structure of different materials connected with solder joints [14], as can be seen in Fig. 3(a). Pierre-Marie *et al.* reported that temperature variations in electronic devices lead to thermal and thermo-mechanical stress concentrations in power modules due to a CTE mismatch between the different packaging materials, resulting in the rupture of the silicon chip or alumina substrate and fatigue rupture of the SnAgCu solder joint parts [14]. We carried out an analysis of the temperature distribution using a simulation model for power semiconductor modules with Al or Al-diamond (10 vol.% of diamond) heat sinks, as can be seen in Figs. 3(b) and (c). According to the data in Figs. 3(b) and (c), the maximum temperature of the silicon chip and the temperature distribution of the module for Al-diamond heat sinks are lower than those of the pure Al heat sink, demonstrating that the thermal energy can be dispersed efficiently in a Al-diamond heat sink compared to one made of pure Al. It is implied that the concentration of the thermal and thermo-mechanical stresses in power semiconductor modules with Al-diamond heat sinks can be restrained compared to that of an Al heat sink.

Table 1 shows the experimentally obtained thermal conductivity of the composite materials. First, the effect of the thermal conductivity in the Al-50 vol.% diamond composite materials with different diamond particle types (MBD4, 6, and 8) has been investigated, as can be seen in Table 1(a), (b), and (c). For these three bulk materials the

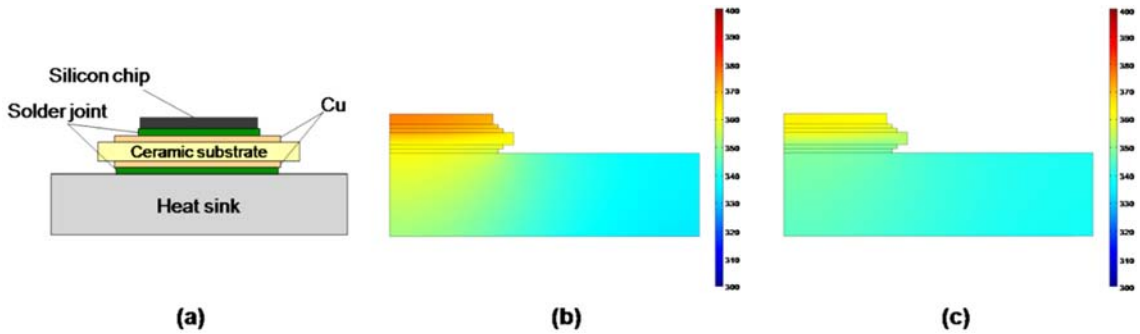

Fig. 3. (a) Typical electronic device architecture. Heat distributions of electronic device module in (b) Al and (c) Al-diamond heat sinks.

Table 1. Some properties of Al-Diamond bulk materials

Sample	Density ($g \cdot cm^{-3}$) (Relative density, %)	Cp ($J \cdot g^{-1} \cdot k^{-1}$)	Thermal diffusivity (mm^2/s)	Thermal conductivity (W/mK)	CTE (10^{-6} °C^{-1})	Ref.
(a) Al-50vol.% MBD4 (37-44 μm)	3.028 (97.4)		98.2	226	-	
(b) Al-50vol.% MBD6 (37-44 μm)	2.980 (95.8)	0.76	104.3	237	11.8	
(c) Al-50vol.% MBD8 (37-44 μm)	2.951 (94.9)		87.3	196	-	
(d) Al-50vol.% MBD6 (25-30 μm)	2.955 (95.0)		64.8	146	-	
(b) Al-50vol.% MBD6 (37-44 μm)	2.980 (95.8)	0.76	104.3	237	118	
(e) Al-50vol.% MBD6 (75-88 μm)	3.040 (97.7)		73.8	171	-	
(f) Al-10vol.% MBD6 (37-44 μm)	2.723 (98.1)	0.87	93.9	223	18.9	
(g) Al-30vol.% MBD6 (37-44 μm)	2.878 (97.7)	0.82	88.3	208	17.3	
(b) Al-50vol.% MBD6 (37-44 μm)	2.980 (95.8)	0.76	104.3	237	11.8	
(i) Pure Al (34 μm)	2.689 (99.5)	0.9	90.4	219	22.9	
Bulk Al	2.698	0.9	-	237	23.5	[6], [7]
Diamond	3.500	0.5	-	1200~2200	1	[5] [8][21][22]

volume fraction of diamond is 50 %. Notice that several materials with the same diamond type and volume fraction have been elaborated, showing good reproducibility of the thermal conductivity results. From this table, it can be seen that:

a) MBD8 composite materials have thermal conductivity lower than that of Al.

b) MBD4 and six other composite materials have thermal conductivity higher than that of Al.

c) MBD6 composite materials show the highest thermal conductivity.

From this set of experiments, the MBD6 diamond powder associated with the Al matrix seems to induce the highest thermal conductivity value for the composite materials. Therefore, we chose this reinforcement type in order to measure the effect of the particle size and volume fraction on the thermal conductivity of the Al-diamond (MBD6) composite material. Second, the effect of the three different diamond particle size ranges has been discussed. Table 1(d), (b), and (e) shows the evolution of the thermal conductivity of the Al-diamond (MBD6) composite materials for three MBD6 particle size ranges: 25-30 μm, 37-44 μm, and 75-88 μm for a volume fraction of 50 %. The thermal conductivity values of 50 vol.% of the MBD6 Al bulk materials with particle size range of 25-30 μm (the smallest one) and 75-88 μm (the largest one) are lower than the thermal conductivity values of the pure Al materials, whereas the thermal conductivity of the materials elaborated with the 37-44 μm range diamond powder is higher than that of pure Al. Finally, the effect of the three different volume fractions of diamond powder (10 %, 30 %, and 50 %) has been investigated with the best diamond type (MBD6) and diamond particle size range (37-44 μm) experimentally found. The thermal conductivity of the composite materials is slightly higher for the 10 vol.% and 50 vol.% of the diamond reinforced sample than for the measured Al bulk materials (219 W/mK), but slightly lower for materials elaborated with 30 vol.% diamond particles, as indicated in Table 1(f), (g), and (b).

In general, the thermal conductivity of the squeeze casted Al-60 vol.% diamond is reported to be 130 W/mK from room temperature up to 50 °C due to the formation of nano carbide [15]. In the case of the sample that was gas pressure infiltrated, AlSi7-60 vol.% diamond is found at 343 W/mK to 375 W/mK. The thermal conductivity of the gas infiltrated sample values cannot be directly compared with the values for our hot pressed pure Al matrix 50 vol.% diamond composite [15]. In any case, the thermal conductivity of the hot pressed Al-diamond composites was not significantly reduced but in fact slightly increased.

The experimentally obtained thermal conductivities were compared with numerical Comsol values and theoretically calculated values, as can be seen in Figs. 4(a) and (b). As can be seen in Fig. 4(a), this behavior was similar to that described by values already calculated by a simple theoretical equation developed from K. Chihiro of Sumitomo Electric Industries [16]. We have obtained much higher values from his practical equation. The demonstrated theoretical thermal conductivity of composites reinforced by different fractions of diamond particles, is listed below [16], where Z is the thermal conductivity of composites and X is the weight fraction of the diamond,

$$Z = 0.2239X^2 - 12.017X + 593.93 \quad (2)$$

According to Chihiro's report, this equation can be used to calculate the thermal conductivity of Al-diamond composites when the composition of the diamond range (X) is 5 % < X < 80 % [16]. However, this equation does not consider the effect of diamond particle size.

On the other hand, Comsol multiphysics simulation always shows a linear increase of thermal conductivity with volume fraction of reinforcement. It must be mentioned that particle size and shape factors are not considered in the equation theoretically calculated by Chihiro, whereas, from

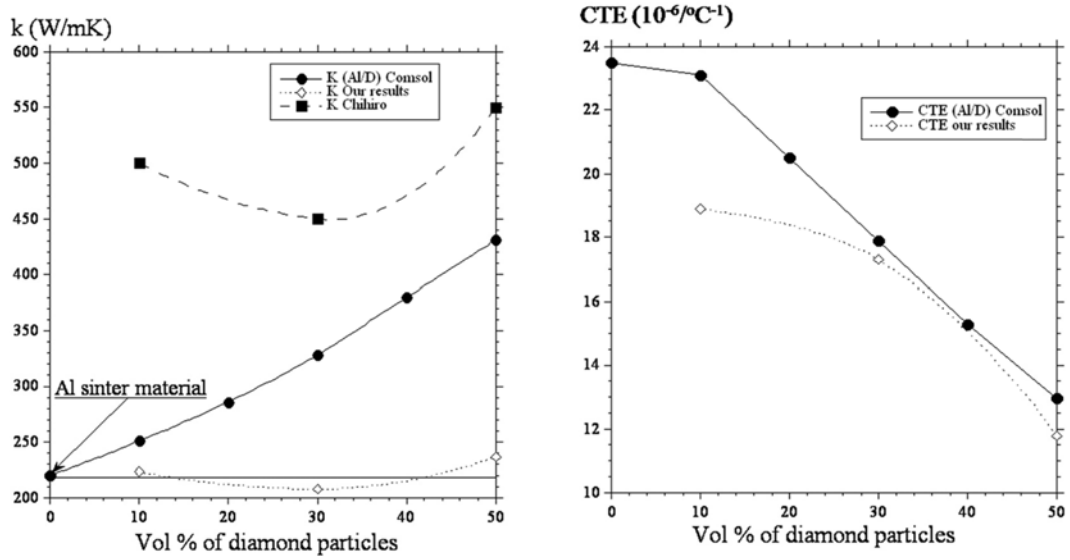

Fig. 4. Theoretically and simulationally calculated thermal conductivities and CTE comparing with experimental values.

the Comsol calculation, we can set particle size with a perfect interface between the Al and diamond particles and a porosity level equal to zero. The thermal conductivity of the Comsol calculated values was found to increase with the increase of diamond addition, but the experimental values did not exactly follow, i.e. it is implied that the obtained composite materials do not have a perfectly bonded interface and include some micropores.

The CTE of the obtained composite materials has been measured at the same time. Figure 4(b) shows the Comsol calculations and the measured CTE of the composite materials with an increased volume fraction of diamond particles. The same behavior can be observed: this is a decrease of the CTE with an increase of the diamond volume fraction. Surprisingly, the CTE values measured for our materials are much lower than the Comsol numerical values, especially for the sample of 10 vol.%. Notice that for real composite materials the CTE has a much lower effect on the porosity level and the quality of the interfacial zone. This reinforcement has to be linked to the matrix, but spot links or continuous links should lead to identical measured CTE values. This behavior is the opposite of that in thermal conductivity measurement, whereas the quality and the size of the interface plays a very important role.

For comparison, pure bulk Al was fabricated under the same experimental conditions as those of the Al-diamond composite, as indicated in Table 1. The pure Al materials show a density of 2.689 g/cm^3, which is close to the density of the reference bulk material (2.698 g/cm^3). However, the thermal conductivity value (219 W/mK) is slightly lower than the reference value (237 W/mK). This small difference may be attributed to experimental errors and/or to the grain boundary, which may be a mixture of alumina and aluminum. In the second case the lower thermal conductivity of alumina (35 W/mK to 40 W/mK) may act as interfacial thermal resistance and may indeed lower the thermal conductivity of the elaborated Al materials.

We have also considered the densification of the obtained composite materials, depending on the different diamond types, particle sizes, and volume fractions. According to the results, the MBD8 diamond reinforced Al matrix composite shows the lowest density among the samples, as indicated in Table 1(a), (b), and (c). This difference may be attributed to the different surface morphology observed by SEM for the three diamond types, as can be seen in Fig. 1. In such a case, a rougher surface of the diamond particle (Fig. 1(f)) is associated with a lower density of the composite. Concerning the size effect of the diamond particles of the final density, a slight increase of the density in the Al-diamond composite materials was observed when the particle size increased, as indicated in Table 1(d), (b), and (e). The densification of the materials containing rigid inclusions has been extensively studied [17,18], usually as a function of the volume fraction of inclusion. It has been shown that the presence of inclusions within a matrix generates transient stresses in the surroundings of any inclusion, leading to a reduction of the densification. In our materials, as indicated in Table 1(d), (b), and (e), the same volume fraction of Al-diamond area of the interface will reduce the differential sintering effect and the amount of porosity close to these interfaces. Such an evolution agrees quite well with the increase of the density according to the diamond particle size. Moreover, at high volume fraction, an interlocking network of inclusions forms, which also inhibits the densification. As a result, differential sintering takes place in the matrix, which leads to the formation of porosity

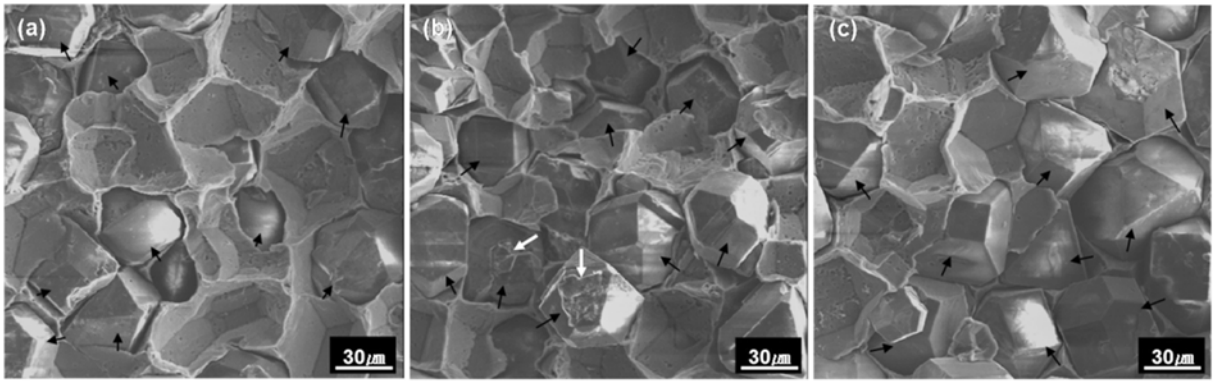

Fig. 5. SEM micrographs of fracture surface of Al-50 vol.% (a) MDB4, (b) MDB6, and (c) MDB8 composite materials. The black arrows and white arrows indicate diamond particles and Al lumps, respectively.

in the region close to the reinforcement particle [18-20].

The fracture surface of the Al-diamond composite materials has been observed by SEM in order to characterize the interfacial zone between the Al matrix and the diamond particle reinforcement. Figure 5 shows the fracture surfaces of the three different types (a) MBD4, (b) MBD6, and (c) MBD8, of the diamond reinforced Al matrix bulk materials fixed in 50 vol.% and an identical particle size range (37-44 mm). Surface ruptures are more or less identical for the three elaborated composite materials, in which adhesive or interfacial fractures are predominant. However, some lumps on the surface of the diamond particles were observed in the case of the Al-MBD6 composite material, which lumps may be attributed to cohesive fracture spots, as shown by the white arrows in Fig. 5(b). At these spots the Al matrix can be linked with the surface of the diamond particles by a diffusion reaction and, therefore, can induce strong chemical bonds between the matrix and reinforcement [21,22].

Figure 6(a) shows evidence of a strongly bonded interface zone between the Al matrix and the diamond particles in the Al-MBD6 composite, even if large cleavage can be observed between the Al matrix and the diamond particles. One spot (see the black arrow in Fig. 6(a)) gives evidence of a bridge linking both constituents. Moreover, the white debris (see the white arrow in Fig. 6(a)) on the surface of the diamond particles is attributed to some Al material that is sticking to the diamond surface. It is implied that these Al materials have reacted with the surface of the diamond, resulting in the formation of enhanced interface bonding. Some vacancies, which were originally positioned diamond particles with no bridging and weak mechanical bonding, have also been observed, as can be seen in Fig. 6(c). For this reason, the thermal conductivity of the Al-MBD6 composite materials showed relatively high values among all samples. By means of spark plasma sintering [23-26], which enables the surface modification of metal/ceramic materials during sintering, it is possible to determine that this sample is an appropriate candidate for fabrication of the Al-diamond composite with highly enhanced thermal properties; we will discuss this sample in our next study.

The effects of sintering temperature, which may affect the formation of different interfaces between the Al and the diamond, were investigated. The Al-10 vol.% diamond bulk materials were employed because of the restrained diamond addition effect. Table 2 shows the thermal conductivity of the obtained Al-10 vol.% diamond bulk materials with different sintering temperatures (600 ˚C, 650 ˚C, and 700 ˚C). There are no significant differences between

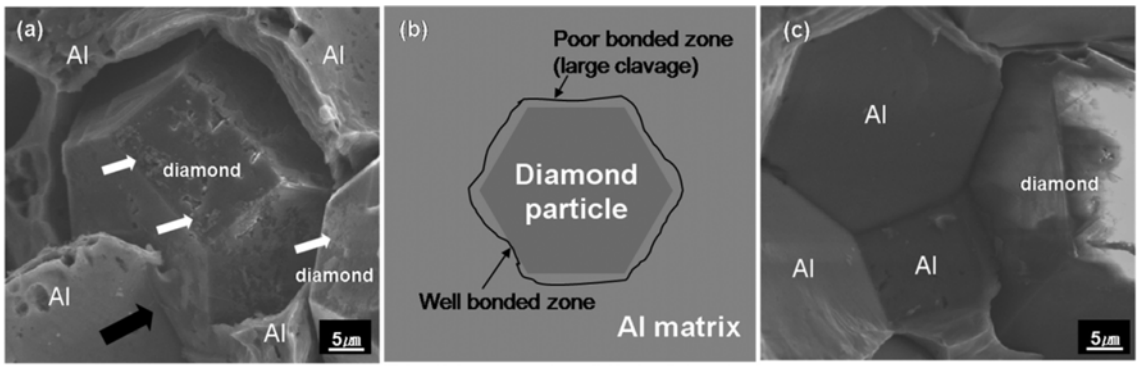

Fig. 6. (a) SEM micrographs and (b) illustrated of fracture surface of Al-50 vol.% MDB6 bulk materials. White and black arrows indicate some Al sticks on the diamond surface and bridge between the Al and diamond. (c) The vacancy which is originally positioned a diamond particle.

Table 2. Some properties of Al-diamond bulk materials depends on the sintering temperature

Sample	Sintering temperature (°C)	Density (g·cm^{-3}) (Relative density, %)	Cp (J·g^{-1}·k^{-1})	Thermal diffusivity (mm^2/s)	Thermal conductivity (W/mK)	CTE (10^{-6} °C^{-1})
(a) Al-10vol.% Diamond	600	2.723 (98.1)		93.9	223	18.9
(b) Al-10vol.% Diamond	650	2.729 (92.6)	0.87	91.0	216	19.4
(c) Al-10vol.% Diamond	700	2.192 (78.8)		30.1	58	18.6
Pure Al	600	2.689 (99.5)	0.9	90.4	219	22.9

the thermal conductivities. However, the thermal conductivity and density of the composite materials sintered at 700 °C were found to have remarkably decreased compared to those of other samples, as indicated in Table 2(c). It is implied that the thermal conductivity can also be affected by the porosity in the Al-diamond bulk materials. The CTE of samples with various sintering temperatures was lower than that of the pure bulk Al, even for high porosity samples (sintered at 700 °C), as indicated in Table 2(c). It may be that the CTE that can be achieved not only continues the bonding but also maintains the point contact. Therefore, in the present work we believe that the parameter of porosity does not have a significant effect as a barrier for the enhancement of CTE.

Here, in order to understand the effect of sintering temperature, we have discussed why the thermal conductivity of the obtained composite materials produced by liquid phase sintering significantly decreased. Figure 7 shows microstructure illustrations of sintered Al-diamond composite materials that were synthesized in solid and liquid sintering regions. In the case of general solid state sintering, as can be seen in Fig. 7(a), the soft Al particles are plastic deformed and some pores between the particles will disappear due to diffusion, with an increase of the sintering temperature and time [17]. Even though some air was trapped between the Al and the diamond particles during solid state sintering, the Al-diamond mixture powders can be highly densified, resulting in well spread thermal energy, as can be seen in Fig. 7(b) and in Table 2(a).

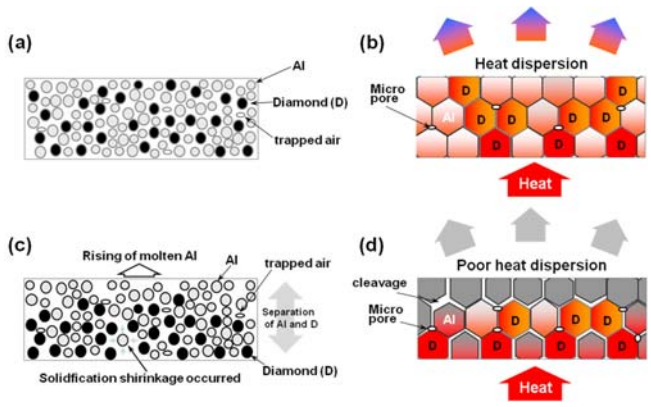

Fig. 7. Illustration of sintering behavior of the Al-diamond mixture powders in (a) solid state and c) liquid phase sintering. (b) and (d) are illustrated microstructures of (a) and (c).

On the other hand, the thermal conductivity and relative density of the composite materials produced by liquid phase sintering were extremely low, compared to the sample sintered in the solid state region, in spite of the increase of the sintering driving force, which was due to the generation of the liquid phase [17]. It is possible that some of the Al liquid phase might have risen during the liquid phase sintering due to the difference of density between the Al and the diamond particles, as can be seen in Fig. 7(c). Many pores were also formed and trapped, accompanied by a relatively high quantity of fume formation due to the melting of the Al. Moreover, lots of micro-cracks occurred in the composite materials due to the solidification shrinkage of the Al, resulting in poor densification and poor spread of thermal energy, as can be seen in Figs. 7(c) and (d).

Figure 8 shows FE-SEM micrographs of the fracture surfaces of Al-10 vol.% diamond composite materials. For the fracture surfaces of the composites sintered at 600 °C and 650 °C, diamond particles seem too strongly implanted in the Al matrix compared to those in the fracture surface that was sintered at 700 °C, as can be seen in Fig. 8. The crevices of the sample sintered at 650 °C were relatively bigger than those in the sample sintered at 600 °C due to partially generated Al liquid phases in the transient sintering region, as can be seen in Figs. 8(a) and (b). Moreover, in the case of the fracture surfaces being sintered at 700 °C, as can be seen in Fig. 8(c), it seems as though the diamond particles had been sprinkled onto the Al matrix and the interface between the Al matrix and the diamond particle was separated. There is a high possibility that some reaction occurred between the defective surfaces of the diamond particles and Al liquid phase during the liquid phase sintering, resulting in some of the Al sticking to the surface of the diamond particles, as can be seen in Fig. 8(f). These reactants that are chemically linked between the Al matrix and the diamond particles may be Al carbide (Al_4C_3) [21, 22,27,28]. In any case, the obtained thermal conductivity was too low even between the chemically linked interface of the Al matrix and the diamond particles. Because some generated gas and solidification shrinkage occurred due to melting and resolidification of Al, the liquid phase sintering was seriously affected, rather than helping the chemically linked interface. However, even if Al_4C_3 is generated during the liquid phase sintering, there may be only a small quantity, and it may be nanosized because the Al oxide

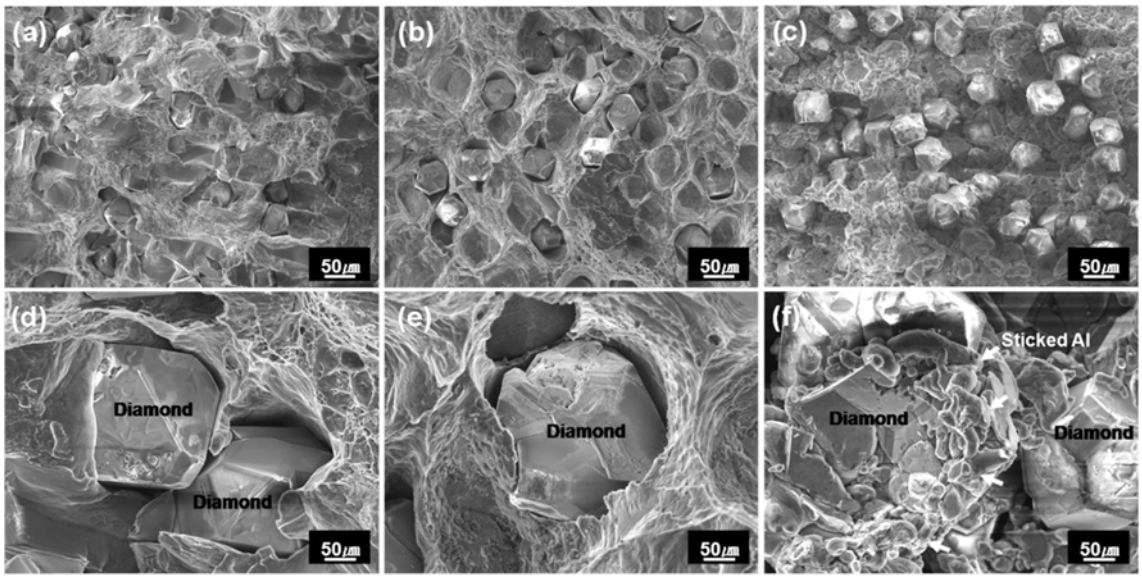

Fig. 8. FE-SEM micrographs of fracture surfaces of Al-10 vol.% diamond composite materials sintered at (a) 600 °C, (b) 650 °C, and (c) 700 °C. (d), (e), and (f) shows their high magnification.

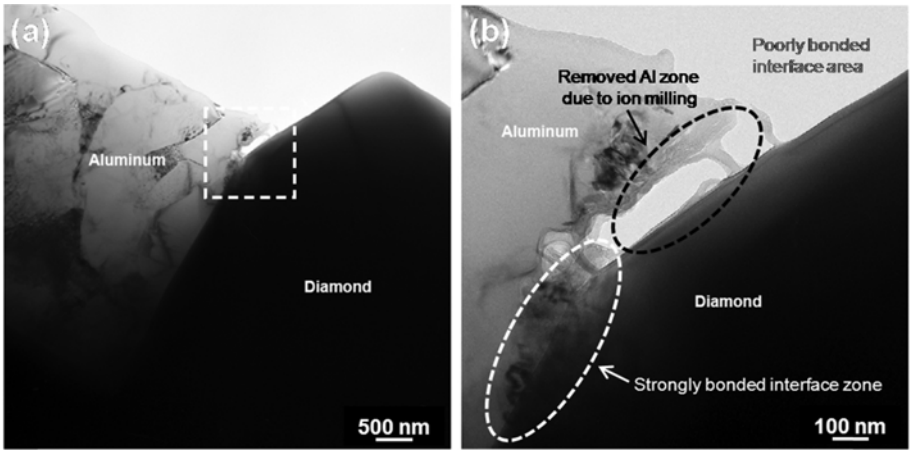

Fig. 9. TEM micrographs of (a) the Al-50 vol.% diamond bulk materials sintered at 600 °C and (b) high magnification of (a). White and black arrows in (b) indicate the strongly bonded and the partially removed Al zone due to ion milling.

layer on the surface of the Al works as a barrier to the reaction between Al and the diamond particles [22,27].

Figure 9 shows TEM micrographs of the Al-50 vol.% diamond bulk materials that showed high thermal conductivity, as indicated in Table 1(b). The Al matrix and the diamond particles are well bonded, as can be seen in Fig. 9(a). Some spaces were observed in the Al matrix due to ion milling (see black circle in Fig. 9(b)). None of the reactants found, such as Al carbide, at the interface between the Al and the diamond particles, were under the TEM resolutions. Deep characterization of the interface between the Al and the diamond will be the subject of our next study. However, it was found that most of the interface in the composites coexists with strongly and poorly bonded zones, as can be seen in Fig. 9(b).

4. CONCLUSIONS

Single crystal diamonds reinforced by Al matrix bulk materials were synthesized and investigated systemically depending on type, size, fraction of diamond, sintering temperature, and atmosphere.

We were able to obtain a homogeneously well dispersed Al-diamond mixture powder by low energy turbular mixing. The obtained Al-diamond bulk materials were highly densified (95 % to 99 %) regardless of diamond type, size, or, volume fraction. The obtained Al-diamond bulk materials show an increment of about 30 % for the thermal conductivity beyond that of pure bulk Al, in spite of the addition of the excellent thermal characteristic of the diamond. This may be due to the poor bonding between the Al

matrix and the diamond particles in the interface. Therefore, an enhanced bonding property between the Al matrix and diamond in the interface should be considered in order to achieve high-performance for thermal management application of Al-diamond bulk materials. Moreover, the thermal conductivity values of samples sintered in the solid and solid-liquid phase transition regions show a thermal conductivity value similar to that of pure bulk Al, but the sample sintered at the liquid phase sintering region showed a value four times lower due to the separation of interfaces between the diamond particles and the Al matrix due to the surface tension of the resolidification of the Al. Hence, it is important to improve not only the densification but also the interface bonding between the Al matrix and the diamond particles in order to achieve high thermal performance for Al-diamond bulk materials.

REFERENCES

1. W. B. Johnson and B. Sonuparlak, *J. Mater. Res.* **5**, 1169 (1993).
2. S. Elomari, R. Boukhili, C. S. Marchi, A. Mortensen, and D. J. Lloyd, *J. Mater. Sci.* **32**, 2131 (1997).
3. V. V. Rao, M. V. K. Murthy, and J. Nagaraju, *Comp. Sci. Technol.* **64**, 2459 (2004).
4. S. Akbulut, Y. Ocak, K. Keslioglu, and N. Marasli, *J. Phy. Chem. Sol.* **70**, 72 (2009).
5. M. Battabyal, O. Beffort, S. Kleiner, S. Vaucher, and L. Rohr, *Dia. Rel. Mater.* **17**, 1438 (2008).
6. P. M. Geffroy, T. Charitier, and J. F. Silvain, *Adv. Eng. Mater.* **7**, 547 (2007).
7. P. M. Geffroy, T. Charitier, and J. F. Silvain, *J. Eur. Ceram. Soc.* **27**, 291 (2007).
8. P. W. Ruch, O. Beffort, S. Kleiner, L. Weber, and P. J. Uggowitzer, *Comp. Sci. Technol.* **66**, 2677 (2006).
9. F. A. Khalid, O. Beffort, U. E. Klotz, B. A. Keller, and P. Gasser, *Dia. Rel. Mater.* **13**, 393 (2004).
10. S. A. Suilik, M. Oshima, T. Tetsui, and K. Hasezaki, *Vacuum* **82**, 1325 (2008).
11. T. Schubert, B. Trindade, T. Weibgarber, and B. Kieback, *Mater. Sci. Eng. A* **475**, 39 (2008).
12. Y. Yamamoto, T. Imai, K. Tanabe, T. Tsuno, Y. Kumazawa, and N. Fujimori, *Dia. Rel. Mater.* **6**, 1057 (1997).
13. K. Yoshida and H. Morigami, *Microelectron. Reli.* **44**, 303 (2004).
14. P. M. Geffroy, T. Charitier, and J. F. Silvain, *Adv. Eng. Mater.* **4**, 400 (2008).
15. O. Beffort, F. A. Khalid, L. Weber, P. Ruch, U. E. Klotz, S. Meier, S Kleiner, *Dia. Rea. Mater.* **15**, 1250 (2006).
16. K. Chihiro, *JP Patent*, JP2000303126 (2000).
17. R. M. German, *Sintering Theory and Practice*, John Wiley & Sons, New York (1996).
18. M. N. Rahaman, *Ceramic Processing and Sintering*, Marcel Dekker, New York (1995).
19. O. Sudre and F. F. Lange, *J. Am. Ceram. Soc.* **75**, 519 (1992).
20. J. Besson, *Mech. Mater.* **19**, 103 (1995).
21. T. Laha, S. Kuchibhatla, S. Seal, W. Li, and A. Agarwal, *Acta Mater.* **55**, 1059 (2007).
22. H. Kwon, M. Estili, K. Takagi, T. Miyazaki, and A. Kawasaki, *Carbon* **47**, 570 (2009).
23. M. Kubota, *J. Alloy. Compd.* **434**, 294 (2007).
24. M. Zadra, F. Casari, L. Girardini, and A. Molinari, *Powder Metall.* **50**, 40 (2007).
25. G. Xie, O. Ohashi, K. Chiba, N. Yamaguchi, M. Song, K. Furuya, and T. Noda, *Mater. Sci. Eng. A* **359**, 384 (2003).
26. M. Omori, *Mater. Sci. Eng. A* **287**, 183 (2000).
27. H. Kwon, D. Park, Y. Park, J.F. Silvain, A. Kawasaki, and Y. Park, *Met. Mater. Int.* **16**, 71 (2010).
28. L. Ci, Z. Ryu, N.Y. Jin-Phillipp, and M. Ruhle, *Acta mater.* **54**, 5367 (2006).